

A Single Image based Head Pose Estimation Method with Spherical Parameterization

Hui Yuan, Mengyu Li, Junhui Hou, and Jimin Xiao

Abstract—Head pose estimation plays a vital role in various applications, e.g., driver-assistance systems, human-computer interaction, virtual reality technology, and so on. In this paper, we propose a novel geometry based algorithm for accurately estimating the head pose from a single 2D face image at a very low computational cost. Specifically, the rectangular coordinates of *only four* non-coplanar feature points from a predefined 3D facial model as well as the corresponding ones automatically/manually extracted from a 2D face image are first normalized to exclude the effect of external factors (i.e., scale factor and translation parameters). Then, the four normalized 3D feature points are represented in spherical coordinates with reference to the uniquely determined sphere by themselves, which are further iteratively refined via 3D morphing to adapt various individuals. Finally, the rotation matrix indicating the head pose is obtained by minimizing the Euclidean distance between the normalized 2D feature points and the 2D re-projections of morphed 3D feature points. Comprehensive experimental results over two popular databases, i.e., *Pointing'04* and *Biwi Kinect*, demonstrate that the proposed algorithm can estimate head poses with higher accuracy and lower run time than state-of-the-art geometry based methods. Even compared with start-of-the-art learning based methods that require large amounts of training data and computational resources or geometry based methods with additional depth information, our algorithm that is training-free still produces comparable performance.

Index Terms—head pose estimation, spherical facial model, face model, morphing, and geometric projection.

I. INTRODUCTION

Head pose estimation is strongly relevant with human-computer interaction, such as driver-assistance systems [1-10], human behavior analysis [11], virtual reality (VR)/ augment reality (AR) based entertainment/education/telepresence. In a driver-assistance system, head pose of the driver is monitored so as to remind the driver to pay attention. For human behavior analysis, head pose estimation is used to assist the estimation of human gaze [12-17] or face recognition [18-19], so as to accurately infer the intentions, desires, feelings, etc., of a person. For VR/AR applications, the desired field of view (FOV) of users can be estimated by head pose estimation. Head pose can be predicted by sensors embedded in head-mounted devices [20] or attached under the skin [21], which are cost and annoying. Therefore, computer vision based head pose estimation with high accuracy and in real-time is considered. Compared with sensor based head

pose estimation, it is more technologically challenging for computer vision based head pose estimation, because the accuracy can be affected by many factors [22], e.g., camera distortion, multisource non-Lambertian reflectance, facial expression, and the presence of accessories like glasses and hats, etc.

Computer vision based head pose estimation needs to transform captured 2D head images into a high level concept of directions [23], i.e., three Euler angles: θ_x (Pitch), θ_y (Yaw) and θ_z (Roll), as shown in Fig. 1. According to [24], we can classify existing computer vision based head pose estimation methods into two categories: learning based methods [1-3] [16] [25-38] that need large amount of training data and computational resources and geometry based methods [4-10] [39-49] that are fast but with a little lower accuracy, see section II for details.

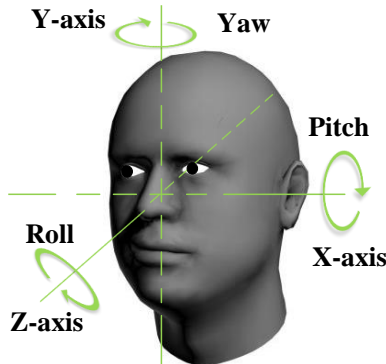


Fig. 1. Head pose represented by three angles, i.e., θ_x (Pitch), θ_y (Yaw) and θ_z (Roll).

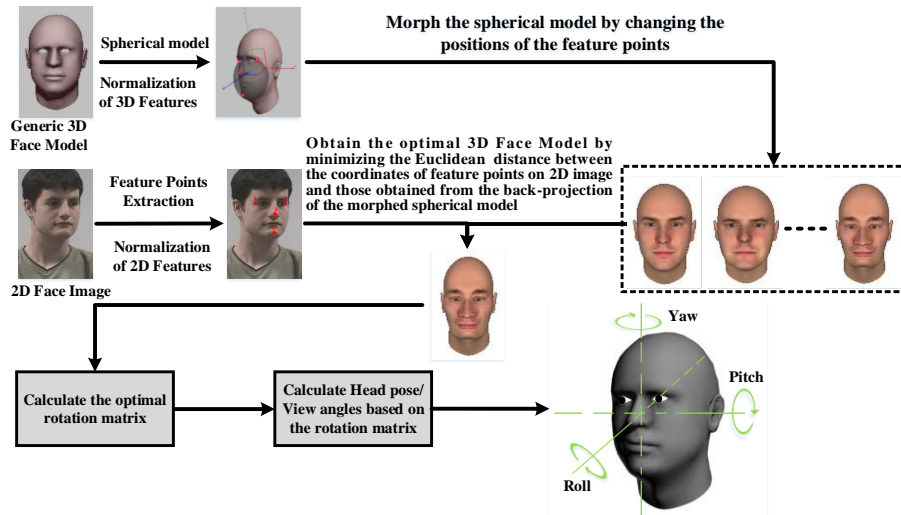


Fig. 2. Illustration of flowchart of the proposed method.

In this paper, as shown in Fig. 2, we propose an accurate geometry based algorithm for estimating the head pose from *a single 2D face image* at a very low computational cost. Specifically, the rectangular coordinates of *only four* non-coplanar feature points from a predefined 3D facial model as well as the corresponding ones automatically/manually extracted from a 2D face image are firstly normalized to eliminate the effect of scale factor and translation parameters, whose effectiveness is theoretically proved. Accordingly, the geometric relationship between the normalized coordinates of feature points in 2D face image and those in 3D facial model can be built by only using a rotation matrix that is denoted by $\mathbf{R} \in \mathbb{R}^{3 \times 3}$.

In order to adapt the various individuals, the four normalized 3D feature points are then represented in spherical coordinates with reference to the uniquely determined sphere by themselves, which are further iteratively refined by varying the azimuth and elevation in the spherical coordinates. Finally, the rotation matrix indicating the head pose is obtained by minimizing the Euclidean distance between the normalized 2D feature points and the 2D re-projections of morphed 3D feature points. Experimental results over two popular databases, i.e., *Pointing'04* and *Biwi Kinect*, demonstrate that the proposed algorithm can estimate head poses with higher accuracy and lower run time than the state-of-the-art geometry based methods.

The rest of this paper is organized as follows. In Section II, related work is introduced. In Section III, the preliminary of the 3D facial model based head pose estimation is presented. Details of the proposed method are given in Section IV. Experimental results and conclusions are given in Section V and VI respectively.

II. RELATED WORK

Learning based methods attempt to find the matching relationship between query face images (usually represented by extracted appearance features) and head positions with the support of huge face datasets [30] in which a sufficient amount of training data uniformly distributed across various pose angles is provided. Mathematically, head poses are estimated by solving a regression or classification problem in the learning based methods. Chutorian *et al.* [1] and [2] trained two support vector regression models based on Localized Gradient Orientation histograms to match the orientation of the driver's head. Fu *et al.* [3] categorized the head pose into 12 gaze zones based on facial features and then used self-learning algorithm and particle filter to estimate the head poses. Ba and Odobez [16] applied a Bayesian probabilistic framework that is solved through particle filtering techniques for head tracking and pose estimation. Tan *et al.* [25] and Fanelli *et al.* [26] present a random forest-based framework to estimation head pose from depth images. Liang *et al.* [27] proposed an improved Hough-voting with random forest via simultaneously changing the weights of leaf votes with L0-regularized optimization and pruning unreliable leaf nodes in the forest. Mukherjee *et al.* [28] and Venturelli *et al.* [29] trained a convolutional neural network (CNN) for human head pose estimation with RGB-D data. Drouard *et al.* [30] used a mixture of linear regression with partially-latent output that learns to map high-dimensional feature vectors (extracted from bounding boxes of faces) onto the joint space of head-pose angles and bounding-box shifts by unsupervised manifold learning so that they can be robustly predicted in the presence of unobservable phenomena. Li *et al.* [31] introduced a tree-structured cascaded adaboost classifiers to detect the multi-view faces with which head poses were then estimated by randomized regression trees. Liu *et al.* [32] provided a synthetic head image dataset which was also used to train a convolutional neural network (CNN) model, and then estimated the head poses by means of a regression method. Rajagopal *et al.* [33] explored transfer learning approaches for efficient multi-view head pose classification with minimal target training data. Foytik *et al.* [34] formulated a two-layer system (coarse/fine) on the assumptions that coarse pose estimation can be performed adequately using supervised linear methods, and fine pose

estimation can be achieved using linear regressive functions if the scope of the pose manifold is limited. Asteriadis *et al.* [35] combined two novel techniques of distance vector fields (DVF) and CNN, respectively based on a local information and holistic appearance information to estimate head pose angles. Sadeghzadeh *et al.* [36] trained a fuzzy system with the input of the facial geometric features, such as the ratios and angles among these feature points, to estimate head pose angles. Riegler *et al.* [37] proposed a Hough Networks (HNs) which combines the Hough Forests with CNN by performing classification and regression simultaneously. Papazov *et al.* [38] introduced a surface patch descriptor-based method for head pose estimation using depth and color information. The performances of learning based methods are usually good, but still limited by the datasets in which uneven illumination, complex background, occlusion, facial expression, gender, and races etc. cannot be considered comprehensively. Besides, the complexity is usually high.

Geometry based methods estimate the head pose by geometrical calculation with feature points. They can be further divided into 2 categories coarsely, i.e. geometry distribution based methods [4] [39-43] and 3D facial model [5-10] [44-49] based methods.

Geometry distribution based methods attempt to estimate the head poses directly from the geometry distribution of feature points on a 2D face image based on a fixed geometrical model. At the early stage, Gee *et al.* [39] compared the proportion between five facial feature points and the length of nose with a fixed value to determine the head direction. Batista [10] and Ji and Hu [40] developed an ellipse model on the face region based on the eye locations and estimate head pose angles by finding the relationship between the head pose angles and these ellipse parameters. Similarly, Yao *et al.* [41] and Narayanan *et al.* [42] also adopted an ellipse-circle model to estimate the head pose. Nikolaidis *et al.* [43] distorted the isosceles triangle formed by the two eyes and the mouth to estimate the head yaw angle. In order to estimate more robust and accurate yaw angle, Narayanan *et al.* [4] proposed an improved generic geometric model based on cylindrical and ellipsoidal models to customize the head pose into 12 different models. However, the distribution of feature points of human faces varies a lot because of gender, races, ages, etc. Therefore, it is hard to estimate various head poses accurately by a fixed geometrical model.

3D facial model based methods estimate the head poses from the correspondence between feature points on a 2D facial image and those on a 3D facial model which can be morphed to match individual facial image. By looking for the projection relation between a 3D facial model and a 2D face image, head pose angles can be calculated from the elements in the rotation matrix directly (see Section III for details). Mbouna *et al.* [5], Fridman *et al.* [6] and Tawari *et al.* [7] solved the rotation matrix to estimate the head pose according to a 3D facial model and corresponding 2D facial feature points directly. Bar *et al.* [8] provided some 3D facial templates to match the 3D point cloud obtained from the depth values so as to estimate head poses by using an iterative closest point (ICP) algorithm. A similar method can also be found in [9]. Xiao *et al.* [44] and Martins *et al.* [45] used the Active Appearance Models (AAM) to obtain the 2D feature points, and then the projection matrix was solved with these 2D feature points and corresponding 3D points. Martins *et al.* [46] proposed a real-time 3D facial model updating method for head pose estimation in which the ICP algorithm is also used to find the

best matching pair of 2D face image and 3D facial model. Li *et al.* [47] proposed a real-time face template reconstruction algorithm based on head pose estimation and tracking in which the ICP algorithm is also used. Meyer *et al.* [48] combined particle swarm optimization (PSO) and the ICP algorithm to estimate the head pose. However, all of them [8-9] [44-48] have used the depth information of 2D face images. Kong and Mbouna [49] estimated head pose angles from a single 2D face image using a 3D face model morphed from a reference face model. But the 3D facial model is morphed only along with one direction.

The performances of the existing methods are good to some extent, but the estimated head pose accuracy should be further improved for practical application with less information and complexity as much as possible.

III. PRELIMINARY: HEAD POSE REPRESENTATION AND 3-D PROJECTION

As shown in Fig. 1, a head can typically rotate around X, Y, and Z axes, and thus, head pose can be represented by three Euler angles, i.e., θ_x (Pitch), θ_y (Yaw) and θ_z (Roll). The three angles correspond to the head actions of nodding, shaking, and rolling, which are helpful for human behavior analysis, gaze and FOV estimation, etc. In a 3D world coordinate, when a point located at (x, y, z) rotates θ_x around the X axis, the resulted coordinate of the point will be

$$(x_X \ y_X \ z_X)^T = \mathbf{R}_X \cdot (x \ y \ z)^T, \quad (1)$$

where

$$\mathbf{R}_X = \begin{bmatrix} 1 & 0 & 0 \\ 0 & \cos \theta_x & -\sin \theta_x \\ 0 & \sin \theta_x & \cos \theta_x \end{bmatrix}. \quad (2)$$

Similarly, when the point rotates θ_y and θ_z around the Y and Z axes, the resulted coordinate will be

$$(x_Y \ y_Y \ z_Y)^T = \mathbf{R}_Y \cdot (x \ y \ z)^T, \quad (3)$$

and

$$(x_Z \ y_Z \ z_Z)^T = \mathbf{R}_Z \cdot (x \ y \ z)^T, \quad (4)$$

respectively, where

$$\mathbf{R}_Y = \begin{bmatrix} \cos \theta_y & 0 & \sin \theta_y \\ 0 & 1 & 0 \\ -\sin \theta_y & 0 & \cos \theta_y \end{bmatrix}, \quad (5)$$

and

$$\mathbf{R}_Z = \begin{bmatrix} \cos \theta_z & -\sin \theta_z & 0 \\ \sin \theta_z & \cos \theta_z & 0 \\ 0 & 0 & 1 \end{bmatrix}. \quad (6)$$

Therefore, for any kind of rotation, the resulted coordinate of the point can be written as:

$$(x_{XYZ} \ y_{XYZ} \ z_{XYZ})^T = \mathbf{R}_X \mathbf{R}_Y \mathbf{R}_Z \cdot (x \ y \ z)^T = \mathbf{R} \cdot (x \ y \ z)^T. \quad (7)$$

where

$$\mathbf{R} = \begin{bmatrix} r_{11} & r_{12} & r_{13} \\ r_{21} & r_{22} & r_{23} \\ r_{31} & r_{32} & r_{33} \end{bmatrix}$$

$$= \begin{bmatrix} \cos \theta_z \cos \theta_y & \cos \theta_z \sin \theta_y \sin \theta_x - \sin \theta_z \cos \theta_x & \cos \theta_z \sin \theta_y \cos \theta_x + \sin \theta_z \sin \theta_x \\ \sin \theta_z \cos \theta_y & \sin \theta_z \sin \theta_y \sin \theta_x + \cos \theta_z \cos \theta_x & \sin \theta_z \sin \theta_y \cos \theta_x - \cos \theta_z \sin \theta_x \\ -\sin \theta_y & \cos \theta_y \sin \theta_x & \cos \theta_y \cos \theta_x \end{bmatrix}. \quad (8)$$

For the rotation matrix \mathbf{R} , as shown in Eq. (8), the three row vectors $\mathbf{r}_1 = (r_{11} \ r_{12} \ r_{13})^T$, $\mathbf{r}_2 = (r_{21} \ r_{22} \ r_{23})^T$, and $\mathbf{r}_3 = (r_{31} \ r_{32} \ r_{33})^T$ have the following relations:

$$\begin{cases} \mathbf{r}_1^T \mathbf{r}_2 = 0 \\ \mathbf{r}_2^T \mathbf{r}_1 = 0 \\ \mathbf{r}_1^T \mathbf{r}_1 = 1 \\ \mathbf{r}_2^T \mathbf{r}_2 = 1 \\ \mathbf{r}_3 = \mathbf{r}_1 \times \mathbf{r}_2. \end{cases} \quad (9)$$

Accordingly, the Euler angles θ_x , θ_y , and θ_z can be calculated as:

$$\theta_x = \tan^{-1} \frac{r_{32}}{r_{33}}, \quad \theta_y = -\tan^{-1} \frac{r_{31}}{\sqrt{r_{32}^2 + r_{33}^2}}, \quad \theta_z = \tan^{-1} \frac{r_{21}}{r_{11}}. \quad (10)$$

According to the pinhole camera model [50], the projection from a 3D facial model to a 2D face image plane can be described as:

$$s \begin{pmatrix} \mu \\ v \\ 1 \end{pmatrix} = \mathbf{A}[\mathbf{R} \ \mathbf{t}] = \begin{bmatrix} \alpha & \gamma & \mu_0 \\ 0 & \beta & \nu_0 \\ 0 & 0 & 1 \end{bmatrix} \begin{bmatrix} \mathbf{r}_1^T & t_1 \\ \mathbf{r}_2^T & t_2 \\ \mathbf{r}_3^T & t_3 \end{bmatrix} \begin{pmatrix} x \\ y \\ z \\ 1 \end{pmatrix}, \quad (11)$$

where s is a scale factor commonly denoted as the projective depth, (μ, v) is the projected pixel coordinates in the image plane, \mathbf{A} is the intrinsic parameter of camera, α and β are scaling factors of the two image axes that depend on the horizontal and vertical focal length of the camera lens, γ is the skew, (μ_0, ν_0) is the coordinate of principal point, and $\mathbf{t} = (t_1 \ t_2 \ t_3)^T$ is the translation vector denoting the distance between camera center and object center with respect to the 3D world coordinate system.

In an ideal camera system without any distortion, we have $\gamma = 0$, $\alpha = \beta$, and $\mu_0 = \nu_0 = 0$. Furthermore, based on the affine perspective assumption [51], when the distance of an object from a camera (corresponding to s and t_3) is much larger than the depth variation (corresponding to the elements in the rotation matrix \mathbf{R}) of the object, Eq. (11) can be simplified as:

$$\begin{pmatrix} \mu \\ v \\ 1 \end{pmatrix} = \begin{bmatrix} \frac{\alpha}{s} r_{11} & \frac{\alpha}{s} r_{12} & \frac{\alpha}{s} r_{13} & \frac{\alpha}{s} t_1 \\ \frac{\alpha}{s} r_{21} & \frac{\alpha}{s} r_{22} & \frac{\alpha}{s} r_{23} & \frac{\alpha}{s} t_2 \\ 0 & 0 & 0 & 1 \end{bmatrix} \begin{pmatrix} x \\ y \\ z \\ 1 \end{pmatrix}. \quad (12)$$

Subsequently, we have

$$\begin{pmatrix} \mu - s't_1 \\ v - s't_2 \\ 1 \end{pmatrix} = s' \begin{bmatrix} r_{11} & r_{12} & r_{13} \\ r_{21} & r_{22} & r_{23} \end{bmatrix} \begin{pmatrix} x \\ y \\ z \end{pmatrix} = s' \begin{bmatrix} \mathbf{r}_1^T \\ \mathbf{r}_2^T \end{bmatrix} \begin{pmatrix} x \\ y \\ z \end{pmatrix}, \quad (13)$$

where $s' = \alpha/s$.

IV. PROPOSED METHOD

According to Eq. (13), with 5 matching pairs of feature points from a 2D face image and a predefined 3D facial model, one can intuitively obtain all the elements of the rotation matrix

by solving linear equations. However, such an intuitive way may produce inaccurate rotation matrix because the pre-defined 3D facial model cannot exactly adapt to all individuals with various genders, races, ages, and facial expressions. To improve the accuracy of the estimated rotation matrix, one alternatively takes more matching pairs of feature points and adopts more advanced regression methods. However, the complexity of extracting a large amount of high-quality matching pairs is very high. Moreover, the head pose angles are only determined by the rotation matrix, and thus the effect of the external factors in Eq. (13) (i.e., the scale factor and translation parameters) has to be excluded. Based on these analysis, we propose a fast and accurate head pose estimation method only based on geometry, in which *only four* non-coplanar feature points are employed. In the proposed method, the effect introduced by the external factors is removed with theoretically guaranteed operations, i.e., coordinate normalization; afterwards, 3D morphing with spherical parameterization is proposed to adapt the 3D facial model to each individual.

A. Feature Point Normalization

Here, the effect of external factors on the estimation of the rotation matrix can be completely excluded by separately performing a normalization operation shown in Fig. 3 to coordinates of 2D and 3D feature points.

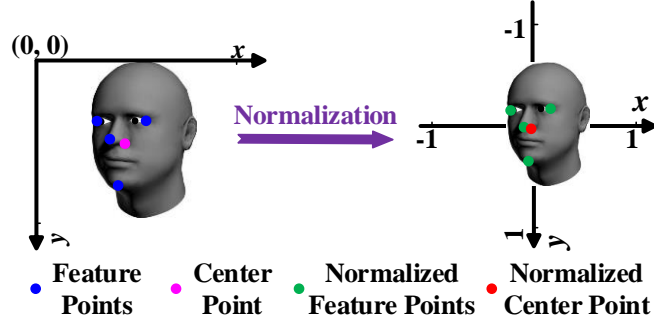


Fig. 3. Normalization of the feature points.

Let $\mathbf{m}_i = (\mu_i \ \nu_i)^T$ and $\mathbf{M}_i = (x_i \ y_i \ z_i)^T$ denote the coordinates of the i -th ($i \in \{1, 2, \dots, N\}$) 2D and 3D feature points respectively, which meet Eq. (13), then we have

$$\mathbf{m}'_i = \mathbf{R}' \mathbf{M}'_i, \quad (14)$$

where $\mathbf{R}' = [\mathbf{r}_1 \ \mathbf{r}_2]^T$, $\mathbf{m}'_i = (\mu'_i \ \nu'_i)^T$, and $\mathbf{M}'_i = (x'_i \ y'_i \ z'_i)^T$ stand for the normalized \mathbf{m}_i and \mathbf{M}_i , respectively:

$$\mathbf{m}'_i = \frac{\mathbf{m}_i - \mathbf{m}_0}{\|\mathbf{m}_i - \mathbf{m}_0\|_2} \quad (15)$$

$$\mathbf{M}'_i = \frac{\mathbf{M}_i - \mathbf{M}_0}{\|\mathbf{M}_i - \mathbf{M}_0\|_2} \quad (16)$$

with \mathbf{m}_0 and \mathbf{M}_0 being the centroids of the feature points:

$$\mathbf{m}_0 = \frac{1}{N} \sum_{i=1}^N \mathbf{m}_i, \quad (17)$$

$$\mathbf{M}_0 = \frac{1}{N} \sum_{i=1}^N \mathbf{M}_i, \quad (18)$$

see appendix for proof.

B. Rotation Matrix Estimation using 3D Morphing with Spherical Parameterization

With the normalized 2D and 3D feature points, the rotation matrix can be obtained directly by solving Eq. (14), i.e., $\mathbf{R}' = \mathbf{m}'_i \mathbf{M}'_i^T (\mathbf{M}'_i \mathbf{M}'_i^T)^{-1}$. However, as aforementioned, inaccurate estimation will be resulted in by using only one pre-defined 3D facial model to fit individuals with various genders, races, ages, and facial expressions. To this end, we propose to iteratively refine the *four* normalized non-coplanar 3D feature points using the 3D morphing with spherical parameterization, and the refined 3D feature points can adapt to each individual better for more accurate estimation. Owing to the advantage of the spherical parameterization of the 3D facial model, the proposed method can morph all the three directions without introducing too much computational complexity to adapt each individual flexibly and accurately.

The four normalized 3D feature points can uniquely determine a sphere (see *Lemma 2* in the *Appendix*). Let $\mathbf{B}'_i = (l \ \phi_i \ \varphi_i)^T$ denote the corresponding spherical coordinate of the i -th 3D feature point, where l is the radius of the sphere, ϕ_i and φ_i are the azimuth and elevation, respectively. The relationship between $\mathbf{B}'_i = (l \ \phi_i \ \varphi_i)^T$ and $\mathbf{M}'_i = (x'_i \ y'_i \ z'_i)^T$ is expressed as

$$\begin{cases} x'_i - x'_o = l \sin \varphi_i \cos \phi_i \\ y'_i - y'_o = l \sin \varphi_i \sin \phi_i \\ z'_i - z'_o = l \cos \varphi_i, \end{cases} \quad (19)$$

where $(x'_o \ y'_o \ z'_o)^T$ is the rectangular coordinate of the center of the sphere. Therefore, individual faces with different characteristics can be adapted by changing the position of these 3D feature points on the sphere, i.e., morphing azimuth (ϕ_i) and elevation (φ_i). For the i -th 3D feature point with the morphing parameters denoted as $\Delta_i = (0 \ \Delta_{i,\phi} \ \Delta_{i,\varphi})^T$, the morphed spherical coordinate is represented as $\widehat{\mathbf{B}}'_i = \mathbf{B}'_i + \Delta_i$, and the corresponding rectangular coordinate $\widehat{\mathbf{M}}'_i = (\widehat{x}'_i \ \widehat{y}'_i \ \widehat{z}'_i)^T$ can be obtained:

$$\begin{cases} \widehat{x}'_i - x'_o = l \sin(\varphi_i + \Delta_{i,\varphi}) \cos(\phi_i + \Delta_{i,\phi}) \\ \widehat{y}'_i - y'_o = l \sin(\varphi_i + \Delta_{i,\varphi}) \sin(\phi_i + \Delta_{i,\phi}) \\ \widehat{z}'_i - z'_o = l \cos(\varphi_i + \Delta_{i,\varphi}). \end{cases} \quad (20)$$

Let $\widehat{\mathbf{M}}'_{i,1}$ denote the initial rectangular coordinate derived from the initial morphing parameter $\Delta_{i,1}$, and the initial re-projected 2D coordinates of $\widehat{\mathbf{M}}'_{i,1}$ be $\widehat{\mathbf{m}}_i(\mathbf{R}^1, \widehat{\mathbf{M}}'_{i,1})$ in which the initial rotation matrix $\mathbf{R}^1 = [\mathbf{r}_1^1 \ \mathbf{r}_2^1 \ \mathbf{r}_3^1]^T$ can be calculated by solving

$$\begin{cases} \mathbf{m}'_i = [\mathbf{r}_1^1 \ \mathbf{r}_2^1]^T \mathbf{M}'_i \\ \mathbf{r}_3^1 = \mathbf{r}_1^1 \times \mathbf{r}_2^1. \end{cases} \quad (21)$$

In order to adapt individual faces by morphing the 3D facial model, the discrepancy between $\widehat{\mathbf{m}}_i(\mathbf{R}^1, \widehat{\mathbf{M}}'_{i,1})$ and \mathbf{m}'_i can be calculated and then minimized iteratively to find the best morphing parameters $\Delta_{i,opt}$:

$$\min_{\Delta_i} \sum_{i=1}^N \|\mathbf{m}'_i - \widehat{\mathbf{m}}_i(\mathbf{R}^1, \widehat{\mathbf{M}}'_{i,k})\|_2^2, \quad (22)$$

where $k \in \{1, \dots, opt\}$ is the iteration index. To ensure that the morphed 3D model is still a human face, we penalize the Euclidean distance between the initial 3D feature points and the morphed ones so that the morphing parameters cannot be arbitrary values, leading to

$$\min_{\Delta_i} \sum_{i=1}^N \|\mathbf{m}'_i - \widehat{\mathbf{m}}_i(\mathbf{R}^1, \widehat{\mathbf{M}}'_{i,k})\|_2^2 + \eta \sum_{i=1}^N \|\widehat{\mathbf{M}}'_{i,k} - \widehat{\mathbf{M}}'_{i,1}\|_2^2, \quad (23)$$

where η is a penalty parameter that controls the deformation of the 3D facial model. The non-linear least squares problem in Eq. (23) can be converted to a linear least squares problem by removing the high order terms of its Taylor expansion with respect to Δ_i . Then the Levenberg-

Marquardt (LM) algorithm [52] that requires a partial derivative of Δ_i is employed to solve the minimization problem iteratively, in which each iteration aims to seek for a suitable damping factor based on the trust region method so as to acquire a reliable update value of Δ_i and decrease the value of objective function to convergence. With the optimal morphing parameter $\Delta_{i,opt}$ obtained, the optimal coordinates of 3D feature points in the rectangular coordinates, i.e., $\hat{\mathbf{M}}'_{i,opt} = (\hat{x}'_{i,opt} \ \hat{y}'_{i,opt} \ \hat{z}'_{i,opt})^T$, can be calculated by

$$\begin{cases} \hat{x}'_{i,opt} - x'_o = l \sin(\varphi_i + \Delta_{i,\varphi,opt}) \cos(\phi_i + \Delta_{i,\phi}) \\ \hat{y}'_{i,opt} - y'_o = l \sin(\varphi_i + \Delta_{i,\varphi,opt}) \sin(\phi_i + \Delta_{i,\phi}) \\ \hat{z}'_{i,opt} - z'_o = l \cos(\varphi_i + \Delta_{i,\varphi,opt}). \end{cases} \quad (24)$$

Finally, the optimal rotation matrix $\mathbf{R}^{opt} = [\mathbf{r}_1^{opt} \ \mathbf{r}_2^{opt} \ \mathbf{r}_3^{opt}]^T$ can be calculated by solving

$$\begin{cases} \hat{\mathbf{M}}'_{i,opt} = \mathbf{M}'_i + \Delta_{i,opt} \\ \mathbf{m}'_i = [\mathbf{r}_1^{opt} \ \mathbf{r}_2^{opt}]^T \hat{\mathbf{M}}'_{i,opt} \\ \mathbf{r}_3^{opt} = \mathbf{r}_1^{opt} \times \mathbf{r}_2^{opt}, \end{cases} \quad (25)$$

where $\hat{\mathbf{M}}'_{i,opt}$ is the i -th normalized 3D feature points that is optimally morphed. The head pose angles can then be calculated by Eq. (10).

V. EXPERIMENTAL RESULTS AND DISCUSSION

To verify the performance of the proposed method, extensive experiments were conducted with a PC equipped with Intel Core i7-7700HQ CPU@2.8GHz, 8GB RAM, and Windows 10 64bits operating system. Two head pose databases were used, i.e., *Pointing'04* [53] and *Biwi Kinect* [54]. The *Pointing'04* database consists of 2790 images of 15 sets of human face with various races, genders, and ages, i.e., 12 sets of male Caucasians, 1 set of female Caucasian, 1 set of female Asian, and 1 set of male Indian. Each set contains 2 series of 93 images with the size of 384×288 at different poses angles. The yaw and pitch angles vary from -90 degree to +90 degree, and there is no roll angle in the *Pointing'04* database. For the *Biwi Kinect* database, there are 15678 images of size 640×480 generated from 20 persons (14 males and 6 females). The head pose angles vary from -75 degree to +75 (yaw), -60 degree to +60 (pitch), and -64 degree to +70 degree (roll).

The 3DsMax software [55] was used to generate a generic 3D facial model as the initial model. The mean absolute error (MAE) of head pose angles between the ground-truth and the estimated ones and the corresponding standard deviation (STD) of the MAEs are computed to evaluate the estimation accuracy. To guarantee that the morphed 3D facial model is also symmetric with the facial symmetry plane, only the azimuth was morphed for the chin and the tip of nose, i.e., $\Delta_{1,\phi} = 0$ and $\Delta_{2,\phi} = 0$; while for the left and right canthus, both the azimuth and elevation were morphed with constraints $\Delta_{3,\varphi} = \Delta_{4,\varphi}$ and $\Delta_{3,\phi} = -\Delta_{4,\phi}$.

V-A Head pose estimation with Manually Labelled 2D Feature Points

We have evaluated the proposed algorithm with manually labelled 2D feature points. As shown in Fig. 4, the four feature points that were manually labelled in 2D face images and used in our algorithm are the chin, the tip of nose on the facial symmetry plane, and the left and right

canthus that are symmetrical with the facial symmetry plane based on the symmetry property of human faces [56]. These four feature points are employed by also considering that they are less sensitive to facial expressions.

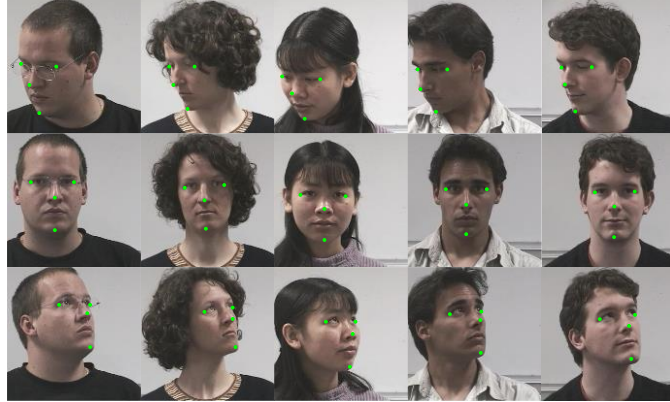


Fig. 4. Feature points used in the experiments, i.e. the chin, the tip of nose, and the left and right canthus.

For the *Pointing'04* database, since we cannot get all of the feature points when the absolute yaw and pitch angles are larger than 45 and 30 degrees respectively, and thus, we only selected 1050 images out of a total 2790 images in the *Pointing'04* database. Similarly, for the *Biwi Kinect* database, we selected 10023 images out of a total 15678 images. The state-of-the-art geometry based method in [49] denoted as ***Kong's TIP2015***, and the estimation method by calculating Eq. (14) directly (denoted as ***without morphing***) were used for comparison.

The estimation errors are listed in Tables I and II for *Pointing'04* and *Biwi Kinect* databases respectively. The plenty factor η in (32), the average iteration numbers of images, and the average run times for images in each image sets of the database are also provided. From Table I (*Pointing'04* database), we can observe that the average MAEs are 6.66 and 7.05 degree for the pitch and yaw angles when the 3D morphing operation is not conducted. For the proposed method (denoted as ***Proposed-MLFP***), the average MAEs are only 3.79 and 3.38 degree for the pitch and yaw angles respectively, while those of ***Kong's TIP2015*** are 7.59 and 4.79 degree respectively. From Table II (*Biwi Kinect* database), we can observe that the average MAEs are 5.63, 3.72, and 2.09 degree for the pitch, yaw, and roll angles when the 3D morphing operation is not conducted. For ***Proposed-MLFP***, the corresponding average MAEs are only 5.04, 3.59, and 2.08 degree respectively, while those of ***Kong's TIP2015*** are 8.71 and 3.62, and 2.11 degree respectively.

Besides, we can also observe that the STDs of MAEs of ***Proposed-MLFP*** are also smaller than those of ***Kong's TIP2015***, which means that the proposed method is more robust for different faces. Although the head pose angles with *more feature points* and a morphed 3D facial model are also used in ***Kong's TIP 2015***, the predefined 3D facial model cannot be morphed along with the x -coordinate and y -coordinate of facial feature points. This means that the inherent structure of the 3D facial model cannot be explored sufficiently to adapt various faces. The advantage of the proposed method over ***Kong's TIP 2015*** is also illustrated in Fig. 5, where the estimation errors of pitch and yaw angles of each tested set of images are compared graphically. Besides, it is seen from Table I and II that the average runtime and average iterations of ***proposed-MLFP*** are smaller than that of ***Kong's TIP2015***.

TABLE I.
ACCURACY COMPARISON OVER THE *POINTING'04* DATABASE

15 Sets	Without morphing			Kong's TIP2015				Proposed-MLFP				
	MAE pitch	MAE yaw	MAE pitch	MAE yaw	Average Runtime	Average Iterations	MAE pitch	MAE yaw	η	Average Runtime	Average Iterations	
1	5.70	8.26	7.24	6.59	0.0232	9.06	3.05	4.06	0.65	0.0121	5.94	
2	6.87	7.51	7.52	4.15	0.0220	8.49	3.87	2.78	1.2	0.0080	3.80	
3	7.39	7.69	9.32	5.55	0.0243	8.94	4.20	4.12	4.9	0.0143	6.23	
4	6.93	5.47	6.79	4.42	0.0243	9.11	3.31	2.94	1.3	0.0116	5.80	
5	6.68	9.05	7.38	8.71	0.0252	10.63	3.63	3.77	0.55	0.0111	5.49	
6	6.42	4.10	7.54	4.17	0.0258	9.91	4.63	2.68	4.5	0.0112	5.31	
7	9.11	9.07	7.77	3.20	0.0241	8.94	3.91	3.52	6.9	0.0080	4.00	
8	8.16	8.27	5.03	3.80	0.0225	8.46	3.58	3.91	1.5	0.0080	3.89	
9	7.21	7.21	5.85	3.28	0.0272	10.29	3.82	3.06	1.4	0.0107	5.09	
10	6.68	5.18	6.77	4.73	0.0346	12.86	3.92	2.63	1.2	0.0179	8.91	
11	5.33	7.76	7.76	5.29	0.0296	11.31	3.56	4.39	2.2	0.0098	4.60	
12	6.55	6.84	13.96	4.51	0.0285	11.03	3.54	3.94	0.6	0.0081	3.54	
13	6.76	6.04	6.65	3.87	0.0308	11.57	3.80	2.52	3.5	0.0063	2.94	
14	5.54	6.34	7.42	6.28	0.0276	11.49	3.91	2.60	5.8	0.0125	5.60	
15	4.65	7.01	6.84	3.33	0.0302	11.86	4.07	3.77	1.2	0.0183	9.46	
Average	6.66	7.05	7.59	4.79	0.0267	10.26	3.79	3.38	-	0.0112	5.37	
STD of MAE	1.11	1.43	2.00	1.50	-	-	0.38	0.66	-	-	-	

TABLE II.
ACCURACY COMPARISON OVER THE *BIWI KINECT* DATABASE

24 Sets	Without Morphing			Kong's TIP2015				Proposed-MLFP						
	MAE Pitch	MAE Yaw	MAE Roll	MAE Pitch	MAE Yaw	MAE Roll	Average Runtime	Average Iteration	MAE Pitch	MAE Yaw	MAE Roll	η	Average Runtime	Average Iteration
1	3.87	5.34	1.54	9.65	4.51	1.68	0.02	13.91	4.29	4.81	1.55	1.30	0.02	5.63
2	6.69	2.88	2.35	11.14	2.77	2.56	0.03	15.60	4.50	3.28	2.35	1.18	0.02	6.42
3	2.96	3.70	2.00	5.19	4.16	2.06	0.02	15.15	4.83	2.86	2.01	1.80	0.01	7.30
4	3.20	4.03	1.62	8.26	3.25	1.52	0.02	14.28	4.39	3.11	1.62	3.50	0.01	6.69
5	2.95	2.67	1.31	4.59	1.97	1.44	0.02	13.23	3.57	2.00	1.33	1.10	0.01	5.02
6	3.87	2.62	1.79	8.90	3.98	1.94	0.03	20.86	3.20	2.16	1.80	1.20	0.01	5.45
7	2.83	2.34	1.28	4.78	3.19	1.38	0.02	14.05	4.37	1.86	1.29	1.40	0.01	5.73
8	7.18	3.52	1.51	9.81	3.42	1.62	0.02	10.52	4.28	3.96	1.53	1.00	0.01	5.60
9	3.55	3.25	1.98	5.60	2.76	2.40	0.02	13.33	3.77	2.52	1.99	1.10	0.01	4.13
10	6.06	4.33	2.69	8.54	3.36	1.78	0.02	8.71	6.08	3.88	2.59	1.20	0.01	4.96
11	2.91	4.28	1.60	3.32	3.12	1.57	0.02	12.40	6.39	5.00	1.60	0.55	0.01	4.44
12	6.84	5.55	3.00	11.39	4.64	2.20	0.02	10.31	6.24	6.02	2.97	1.25	0.01	4.48
13	8.63	2.85	0.91	8.78	2.77	0.78	0.02	10.89	6.75	3.51	0.92	1.10	0.01	4.15
14	3.25	2.30	1.48	3.55	2.55	1.71	0.02	15.81	2.97	2.01	1.47	1.20	0.01	5.56
15	3.15	4.08	1.87	6.15	3.91	1.85	0.02	8.75	3.38	4.38	1.87	1.40	0.01	3.21
16	15.42	4.30	1.65	8.23	3.78	1.68	0.01	7.73	10.10	4.27	1.62	0.40	0.01	3.57
17	4.78	5.26	2.12	11.78	5.14	2.05	0.01	3.72	4.59	5.43	2.09	1.05	0.01	3.32
18	4.49	2.81	3.23	5.70	3.68	3.52	0.03	17.38	4.28	2.73	3.24	1.40	0.01	6.01
19	3.00	2.76	3.02	6.99	3.38	3.49	0.03	19.16	3.21	2.60	3.02	1.50	0.02	5.93
20	5.52	2.60	2.15	5.76	2.75	2.39	0.02	17.56	4.92	2.81	2.16	1.50	0.01	5.05
21	9.58	5.46	3.19	14.62	5.37	3.53	0.02	17.32	9.53	5.38	3.19	1.40	0.02	6.30
22	6.23	4.89	2.57	12.10	5.44	2.58	0.02	13.61	7.42	4.76	2.58	2.00	0.02	7.75
23	13.52	4.49	3.67	23.49	3.39	3.45	0.02	10.78	4.31	4.10	3.65	1.00	0.02	5.07
24	4.74	2.92	1.58	10.74	3.65	1.54	0.02	17.53	3.65	2.83	1.59	1.10	0.01	4.38
Average MAE	5.63	3.72	2.09	8.71	3.62	2.11	0.02	13.44	5.04	3.59	2.08	-	0.01	5.26
STD of MAE	3.33	1.07	0.72	4.33	0.90	0.75	-	-	1.89	1.21	0.72	-	-	-

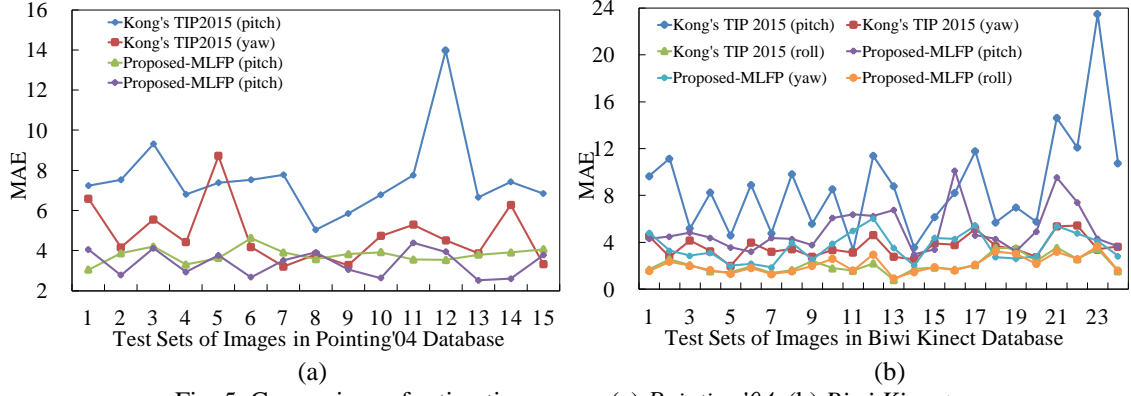


Fig. 5. Comparison of estimation errors, (a) *Pointing '04*, (b) *Biwi Kinect*.

Head pose estimation with automatically labelled 2D feature points

We also have evaluated the proposed algorithm with automatically labelled 2D feature points. The Deep Convolutional Network Cascade (D-CNN) [57] was adopted to detect feature points on 2D face images, in which five feature points, i.e., the two focal points of the eye, the tip of nose, and the two corners of the mouth, can be detected. Since only four feature points are needed in the proposed method, the two focal points of the eye, the tip of nose, and the midpoint of the two corners of the mouth are selected, as shown in the green points in Fig. 6.



Fig. 6. The distribution of the midpoint of two mouth corners and the actual midpoint (the red point) of mouth.

TABLE III.
ACCURACY COMPARISON BASED ON *POINTING '04* DATABASE

15 Sets	Without morphing with D-CNN		Without morphing with AAM		Proposed-MLFP		Proposed-ALFP with D-CNN		Proposed-ALFP with AAM		Kong's TIP2015 with AAM	
	MAE	MAE	MAE	MAE	MAE	MAE	MAE	MAE	MAE	MAE	MAE	MAE
	pitch	yaw	pitch	yaw	pitch	yaw	pitch	yaw	pitch	yaw	pitch	yaw
1	14.09	10.54	8.69	17.31	3.05	4.06	10.09	6.36	8.39	17.26	7.75	9.15
2	12.94	4.94	10.65	10.27	3.87	2.78	3.62	4.09	7.27	5.53	8.92	3.98
3	12.94	4.94	13.07	9.34	4.20	4.12	5.96	4.86	13.79	4.02	16.85	5.16
4	5.31	4.10	13.47	14.23	3.31	2.94	3.25	3.52	11.32	7.27	8.92	3.98
5	25.74	7.53	17.04	15.62	3.63	3.77	11.77	8.73	12.78	16.02	21.33	13.65
6	15.07	5.01	13.66	7.41	4.63	2.68	6.38	4.63	12.49	6.93	10.49	4.28
7	9.49	3.87	9.92	5.19	3.91	3.52	8.35	3.51	9.28	4.23	11.03	4.98
8	6.05	4.14	15.44	5.32	3.58	3.91	4.40	4.00	13.39	6.18	12.07	3.33
9	8.47	7.89	9.33	7.40	3.82	3.06	7.30	7.59	8.80	5.92	9.74	5.74
10	9.58	5.08	10.50	5.64	3.92	2.63	8.96	4.26	8.60	5.40	5.03	3.41
11	12.55	4.39	9.34	5.64	3.56	4.39	4.44	4.68	8.53	5.85	10.11	5.28
12	17.75	6.41	9.92	11.06	3.54	3.94	2.80	7.02	4.93	9.70	20.41	6.98
13	8.33	5.95	5.45	4.98	3.80	2.52	7.55	5.62	4.11	4.44	6.92	5.05
14	13.51	6.36	11.02	8.63	3.91	2.60	5.80	5.31	10.89	5.04	11.66	7.30
15	15.77	2.97	13.47	8.67	4.07	3.77	11.04	3.25	12.98	7.60	11.33	5.41
Average MAE	12.51	5.61	11.40	9.11	3.79	3.38	6.78	5.16	9.84	7.43	11.50	5.85
STD of MAE	5.13	1.93	2.95	3.95	0.38	0.66	2.84	1.62	3.02	4.02	4.64	2.66

Table III (*Pointing '04* database) compares the estimation errors between the proposed method with automatically labelled 2D feature points (denoted as **Proposed-ALFP with D-CNN**) and Kong's TIP2015 with AAM. The proposed method shows significantly lower MAE than Kong's TIP2015 with AAM for most test sets.

CNN) and that with manually labelled feature points. We can see that the MAEs of ***Proposed-ALFP with D-CNN*** are almost larger than those of ***Proposed-MLFP*** for all the tested images. In details, Fig. 7 shows the trend of the estimation errors of pitch and yaw angles of tested images of each set. By observing Fig. 7, it is obvious that accuracy of the ***Proposed-ALFP with D-CNN*** is considerably fluctuated compared with that of the ***Proposed-MLFP***. The reasons are that the midpoint of the two corners of the mouth may not be always located on the actual midpoint of mouth especially when the head pose and the facial expression is changed, as shown in the red points in Fig. 6.

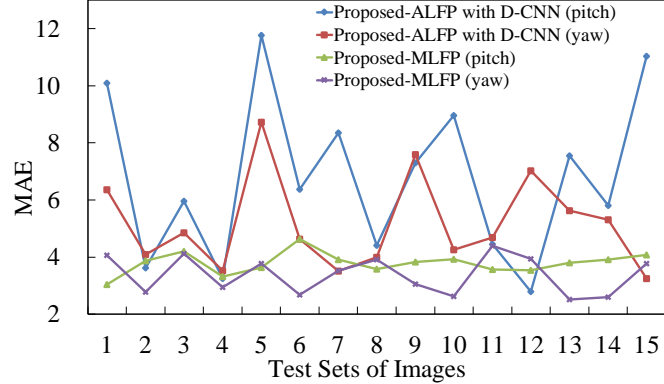


Fig. 7. Estimation errors of yaw and pitch angles of tested images of each person.

For fair comparisons with ***Kong's TIP2015*** [49], we also used the AAM method [58] that was adopted by ***Kong's TIP2015*** to extract 2D feature points. The corresponding estimation errors are also given in Table III, from which we can observe that the accuracy of the ***Proposed-ALFP with D-CNN*** is higher than that of the ***Proposed-ALFP with AAM*** because D-CNN can extract feature points from 2D face images with higher accuracy than AAM. Besides, we can also observe that the average MAE of pitch angle of the ***Proposed-ALFP with AAM*** is smaller than that of ***Kong's TIP2015 with AAM***, but the average MAE of yaw angle of the proposed method is larger. The reason is that in ***Kong's TIP2015 with AAM*** more horizontally arranged feature points are used.

Moreover, Fig. 8 shows the convergence of estimation errors with respect to iterations. From this figure, we can observe that the estimation errors of the ***Proposed-MLFP*** converges faster than that of the ***Proposed-ALFP with AAM***, while the converged estimation error of the ***Proposed-ALFP with AAM*** is larger than that of the ***Proposed-MLFP***, which means that the performance of the proposed method depends on the accuracy of the 2D feature points.

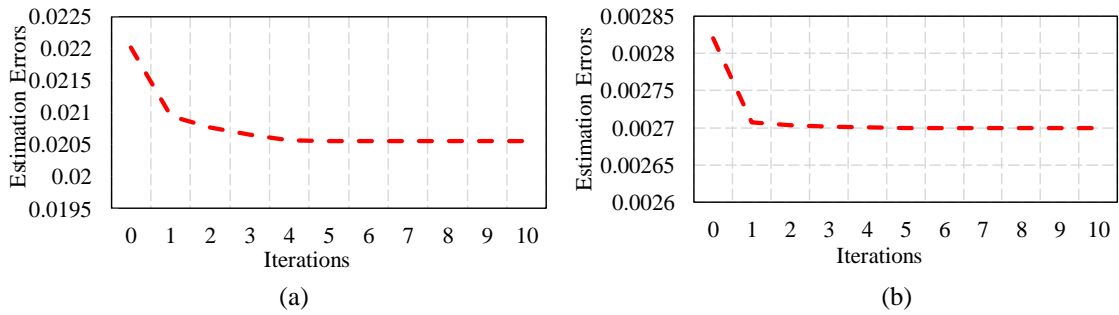


Fig. 8. Estimation errors with respect to iterations, (a) ***Proposed-ALFP with AAM***, (b) ***Proposed-MLFP***.

For the ***Biwi Kinect*** database, the estimation errors of all the 24 sets are also compared in Table IV. Since it is hard to get all of the feature points when the absolute yaw and pitch angles are too large, we only selected 7466 images out of a total 15678 images so as to obtain the four feature points accurately by D-CNN [57] and AAM [58]. From Table IV, we can observe that

the average MAEs of pitch, yaw, and roll angles of ***Proposed-ALFP with AAM*** are 6.70, 5.20, and 1.91, respectively, while those of ***Kong's TIP2015 with AAM*** are 10.36, 6.11, and 1.93, respectively. We can also observe that the STDs of MAEs of the ***Proposed-ALFP with AAM*** are 3.55, 1.72, and 0.81 respectively, which are smaller than those of ***Kong's TIP2015 with AAM***. Besides, the average MAEs of pitch, yaw, and roll angles of ***Proposed-ALFP with D-CNN*** are 5.94, 6.64, and 2.08, while the corresponding STDs of the MAEs are only 1.39, 1.21, and 0.73.

TABLE IV.
ESTIMATION ERRORS OF PITCH AND YAW ANGLES OF ALL THE 24 SETS IN BIWI KINECT DATABASE

24 Sets	Without Morphing with AAM			Proposed-ALFP with D-CNN			Proposed-ALFP with AAM					Kong's TIP2015 with AAM					
	MAE Pitch	MAE Yaw	MAE Roll	MAE Pitch	MAE Yaw	MAE Roll	MAE Pitch	MAE Yaw	MAE Roll	η	Average Runtime	Average Iterations	MAE Pitch	MAE Yaw	MAE Roll	Average Runtime	Average Iterations
	1	4.43	2.78	1.21	5.09	7.46	0.99	4.49	3.04	1.21	1.30	0.01	4.79	10.85	3.85	1.35	0.01
2	10.78	5.80	2.67	5.65	6.58	1.76	8.58	6.50	2.65	1.18	0.01	4.66	10.53	9.62	2.76	0.03	8.78
3	5.41	7.19	2.95	4.53	6.65	3.83	4.00	6.55	2.96	1.80	0.02	5.29	12.00	7.28	3.05	0.02	4.38
4	5.30	6.49	2.16	4.77	6.21	1.92	5.60	6.60	2.16	3.50	0.07	7.01	8.18	9.26	2.21	0.05	9.21
5	5.83	5.65	1.30	3.96	7.45	1.29	4.98	5.86	1.30	1.10	0.03	4.18	9.02	6.62	1.53	0.11	8.56
6	6.38	3.25	1.52	5.72	5.73	2.23	5.04	4.16	1.51	1.20	0.01	3.06	6.71	3.37	1.58	0.01	6.05
7	10.28	24.14	1.89	6.07	8.32	1.63	4.78	5.12	1.37	1.40	0.01	4.12	5.13	6.42	1.02	0.02	6.86
8	13.12	6.86	2.97	4.62	8.16	2.12	7.50	7.79	2.92	1.00	0.02	5.33	18.23	7.78	3.05	0.12	9.71
9	11.57	6.46	1.22	8.33	7.03	2.67	9.49	8.28	1.24	1.10	0.01	4.38	8.67	8.06	1.53	0.11	11.60
10	5.07	3.77	1.65	6.50	3.38	1.62	4.78	3.50	1.68	1.20	0.01	4.61	9.12	5.31	1.45	0.06	5.87
11	20.36	6.59	2.44	7.69	6.96	2.05	21.11	7.92	2.45	0.55	0.01	3.67	15.77	9.07	1.93	0.14	13.42
12	4.56	4.43	2.16	5.12	6.93	2.37	4.73	4.66	2.11	1.25	0.03	5.79	19.40	5.34	1.79	0.13	8.98
13	6.53	2.44	0.89	4.22	5.18	1.19	4.35	2.88	0.90	1.10	0.01	4.82	10.97	4.09	0.82	0.01	5.57
14	9.94	4.50	1.09	3.99	6.91	0.85	8.05	6.32	1.08	1.20	0.01	3.98	4.88	6.35	1.28	0.07	10.81
15	3.34	3.81	1.94	4.14	5.47	2.48	3.36	4.06	1.94	1.40	0.01	3.57	6.28	4.55	1.74	0.04	7.68
16	8.23	3.59	1.80	5.72	6.50	2.64	6.55	4.37	1.76	0.40	0.01	4.11	9.10	5.17	1.80	0.05	8.12
17	5.10	5.49	1.63	6.53	6.08	2.27	4.66	5.53	1.61	1.05	0.01	3.24	12.38	7.68	1.41	0.01	2.50
18	10.03	4.24	1.79	6.71	7.05	2.27	9.07	4.60	1.79	1.40	0.01	5.16	11.53	6.89	1.84	0.04	5.96
19	5.74	6.33	2.41	6.51	8.71	1.95	5.63	6.81	2.41	1.50	0.01	3.12	6.74	5.92	2.99	0.03	9.24
20	5.99	3.65	1.51	7.28	5.88	2.00	4.82	3.73	1.51	1.50	0.01	4.30	3.87	5.53	1.83	0.01	6.29
21	9.50	4.01	4.36	8.22	7.13	3.61	8.60	3.99	4.34	1.40	0.01	4.52	13.22	3.96	4.31	0.03	7.00
22	6.10	2.18	0.70	8.32	4.92	2.33	5.32	2.43	0.69	2.00	0.03	4.92	4.43	3.13	0.86	0.01	1.83
23	8.26	2.67	2.74	6.17	6.33	2.66	7.22	3.30	2.71	1.00	0.01	3.25	22.56	3.26	2.53	0.06	11.88
24	8.95	6.52	1.67	6.78	8.45	1.21	8.02	6.85	1.66	1.10	0.01	3.15	9.04	8.08	1.74	0.01	10.17
Average	7.95	5.54	1.94	5.94	6.64	2.08	6.70	5.20	1.91	-	0.01	4.38	10.36	6.11	1.93	0.05	7.85
STD of MAE	3.70	4.26	0.81	1.39	1.21	0.73	3.55	1.72	0.81	-	-	-	4.80	1.97	0.82	-	-

Furthermore, in order to evaluate the performance of the proposed method comprehensively, we have compared the proposed method with some learning based methods (that need additional training processing and a large amount of training data), i.e., the improved Hough-voting with random forest [27], the DVF and CNN-based method in [35], the fuzzy systems based method in [36], and the ellipsoidal model based geometry method in [42], and ***Kong's TIP2015*** with AAM [49] in Table V for the Pointing'04 database, from which it can be observed that the MAE of the pitch and yaw angle of ***Proposed-MLFP*** is the smallest, while the MAE of the pitch and yaw angle of ***Proposed-ALFP with D-CNN*** is comparable to the start-of-the-art learning based methods.

For the Biwi Kinect database, we also compared the proposed method with some recent learning based and geometry based methods, including HNs based method in [37], surface patch descriptor-based method in [38], real-time 3D facial model updating based method in [46], the face template reconstruction based method in [47], PSO and the ICP algorithm in [48], CNN based inverse regressions in [60] and Recurrent Neural Network (RNN) based method [61]. The corresponding results are listed in Table VI, from which we can observe that the

proposed method is comparable with those methods; while, **in particular, the proposed method that is training-free and only needs a 2D face image produces the best roll angle.**

TABLE V.

COMPARISONS WITH RECENT METHODS OVER *POINTING'04* DATABASE

Classification	Methods	MAE of Pitch Angle	MAE of Yaw Angle
Learning based Methods	Random Forest [27] (<i>ACCV2016</i>)	5.4	4.4
	DVF and CNN [35] (<i>IJCV2014</i>)	4.3	5.18
	Fuzzy System [36] (<i>IST2016</i>)	6.98	6.04
Geometry based Methods	Ellipsoidal Model [42] (<i>TIIS2014</i>)	NA	6.82
	<i>Kong's TIP2015</i> [49] with AAM	11.5	5.85
	<i>Proposed-ALFP</i> with AAM	9.84	7.43
	<i>Proposed-ALFP</i> with D-CNN	6.78	5.16
	<i>Proposed-MLFP</i>	3.79	3.38

TABLE VI.

COMPARISONS WITH RECENT METHODS OVER THE *BIWI KINECT* DATABASE

Classifications	Methods	MAE of Pitch Angle	MAE of Yaw Angle	MAE of Roll Angle
Learning based methods	Hough Networks [37] (<i>BMVC2014</i>)	6.68	3.84	4.33
	Surface Patch Descriptor [38] (<i>ICCV2015</i>)	3	3.9	2.5
	CNN based Inverse Regressions [60] (<i>CVPR2017</i>)	4.68	3.12	3.07
	RNN based method [61] (<i>CVPR2017</i>)	3.48	3.14	2.6
Geometry based methods with depth information	Real-time Model Updating [46] (<i>3DV2014</i>)	2.54	2.57	3.62
	Face Template Reconstruction [47] (<i>TPAMI2016</i>)	3.1	3.3	2.9
	PSO+ICP (2015) [48] (<i>ICCV2015</i>)	2.1	2.1	2.4
Geometry based methods without depth information	<i>Kong's TIP2015</i> [48] with AAM	10.36	6.11	1.93
	<i>Proposed-ALFP</i> with D-CNN	5.94	6.64	2.08
	<i>Proposed-ALFP</i> with AAM	5.7	5.2	1.91
	<i>Proposed-MLFP</i>	5.04	3.59	2.08

VI. CONCLUSION

We have presented a novel head pose estimation method based on the geometrical relationship between 4 non-coplanar feature points in 2D face image and those in a predefined 3D facial model. The coordinates of the 4 feature points are first converted to normalized coordinates so as to remove the influence of the scale and translation parameters in the 3D projection. Then the coordinates of feature points in the 3D facial model are transformed into the spherical coordinates and morphed to adapt various distributions of feature points of individual faces. The optimal morphing parameters with which the rotation matrix as well as head pose angles can be calculated are then found by LM algorithm. Experimental results demonstrate that the accuracy of the roll angle estimated by the proposed method is the best when comparing with all the existing geometry and learning based methods. For the pitch and yaw angles, the accuracy of the proposed method is the best when comparing with existing geometry based method, and is comparable with existing learning based methods that made used of depth information additionally.

APPENDIX

Proof of Eq. (14):

According to (13), the relationships between \mathbf{m}_0 and \mathbf{M}_0 , and between \mathbf{m}_i and \mathbf{M}_i can be respectively written as

$$\begin{cases} \mathbf{m}_0 - s'\mathbf{t}' = s'\mathbf{R}'\mathbf{M}_0 & \text{(i)} \\ \mathbf{m}_i - s'\mathbf{t}' = s'\mathbf{R}'\mathbf{M}_i, & \text{(ii)} \end{cases} \quad (26)$$

where $\mathbf{t}' = (t_1 \ t_2)^T$. By subtracting Eq. (26)–(ii) with Eq. (26)–(i), we have

$$\mathbf{m}_i - \mathbf{m}_0 = s'\mathbf{R}'(\mathbf{M}_i - \mathbf{M}_0). \quad (27)$$

Therefore, based on Eq. (15), \mathbf{m}'_i can be rewritten as

$$\mathbf{m}'_i = \frac{s'\mathbf{R}'(\mathbf{M}_i - \mathbf{M}_0)}{\|\mathbf{m}_i - \mathbf{m}_0\|_2}. \quad (28)$$

Furthermore, substitute $\mathbf{M}_i - \mathbf{M}_0$ by $\mathbf{M}'_i \cdot \|\mathbf{M}_i - \mathbf{M}_0\|_2$ in terms of Eq. (16), Eq. (28) can be represented as

$$\mathbf{m}'_i = \frac{s'\mathbf{R}'\mathbf{M}'_i \cdot \|\mathbf{M}_i - \mathbf{M}_0\|_2}{\|\mathbf{m}_i - \mathbf{m}_0\|_2}. \quad (29)$$

Accordingly, $s' \cdot \|\mathbf{M}_i - \mathbf{M}_0\|_2$ must be proved to be equal to $\|\mathbf{m}_i - \mathbf{m}_0\|_2$.

Let d_0 and D_0 denote the $\|\mathbf{m}_i - \mathbf{m}_0\|_2$ and $s' \cdot \|\mathbf{M}_i - \mathbf{M}_0\|_2$ respectively, based on Eq. (27), we have

$$\begin{aligned} \frac{d_0}{D_0} &= \frac{\|\mathbf{m}_i - \mathbf{m}_0\|_2}{s' \cdot \|\mathbf{M}_i - \mathbf{M}_0\|_2} \\ &= \frac{\|s'\mathbf{R}'(\mathbf{M}_i - \mathbf{M}_0)\|_2}{s' \cdot \|\mathbf{M}_i - \mathbf{M}_0\|_2} \\ &= \frac{\|\mathbf{R}'(\mathbf{M}_i - \mathbf{M}_0)\|_2}{\|\mathbf{M}_i - \mathbf{M}_0\|_2}, \end{aligned} \quad (30)$$

where $\|\mathbf{R}'(\mathbf{M}_i - \mathbf{M}_0)\|_2$ can be represented as

$$\begin{aligned} \|\mathbf{R}'(\mathbf{M}_i - \mathbf{M}_0)\|_2 &= \sqrt{(\mathbf{M}_i - \mathbf{M}_0)^T \mathbf{R}'^T \mathbf{R}' (\mathbf{M}_i - \mathbf{M}_0)} \\ &= \sqrt{(\mathbf{M}_i - \mathbf{M}_0)^T [\mathbf{r}_1 \ \mathbf{r}_2] \begin{bmatrix} \mathbf{r}_1^T \\ \mathbf{r}_2^T \end{bmatrix} (\mathbf{M}_i - \mathbf{M}_0)} \\ &= \sqrt{(\mathbf{M}_i - \mathbf{M}_0)^T (\mathbf{r}_1 \mathbf{r}_1^T + \mathbf{r}_2 \mathbf{r}_2^T) (\mathbf{M}_i - \mathbf{M}_0)}. \end{aligned} \quad (31)$$

Let \mathbf{C} denotes $\mathbf{r}_1 \mathbf{r}_1^T + \mathbf{r}_2 \mathbf{r}_2^T$, we have

$$\begin{aligned} \mathbf{r}_2^T \mathbf{C} &= \mathbf{r}_2^T (\mathbf{r}_1 \mathbf{r}_1^T + \mathbf{r}_2 \mathbf{r}_2^T) \\ &= \mathbf{r}_2^T \mathbf{r}_1 \mathbf{r}_1^T + \mathbf{r}_2^T \mathbf{r}_2 \mathbf{r}_2^T. \end{aligned} \quad (32)$$

Because $\mathbf{r}_2^T \mathbf{r}_1 = 0$ and $\mathbf{r}_2^T \mathbf{r}_2 = 1$, Eq. (32) can be derived as

$$\mathbf{r}_2^T \mathbf{C} = \mathbf{r}_2^T. \quad (33)$$

That is to say \mathbf{C} must be an identity matrix. Accordingly, Eq. (30) can be rewritten as

$$\frac{d_0}{D_0} = \frac{\sqrt{(\mathbf{M}_i - \mathbf{M}_0)^T \mathbf{C} (\mathbf{M}_i - \mathbf{M}_0)}}{\sqrt{(\mathbf{M}_i - \mathbf{M}_0)^T (\mathbf{M}_i - \mathbf{M}_0)}} = 1. \quad (34)$$

Proof end.

Lemma 2: A sphere can be uniquely determined by 4 non-coplanar points.

Proof: For a sphere centered at $(x_0 \ y_0 \ z_0)$ with radius of l , the equation of any point $(x \ y \ z)$ on the sphere can be written as,

$$(x - x_0)^2 + (y - y_0)^2 + (z - z_0)^2 = l^2. \quad (35)$$

Therefore, in order to determine a sphere uniquely, the set of parameters $\{x_0, y_0, z_0, l\}$ must be calculated uniquely. When there are 4 non-coplanar points, i.e., $(x_i \ y_i \ z_i), i \in \{1,2,3,4\}$, we should prove that there is a unique solution for the following equations:

$$\begin{cases} (x_1 - x_0)^2 + (y_1 - y_0)^2 + (z_1 - z_0)^2 = l^2 & \text{(i)} \\ (x_2 - x_0)^2 + (y_2 - y_0)^2 + (z_2 - z_0)^2 = l^2 & \text{(ii)} \\ (x_3 - x_0)^2 + (y_3 - y_0)^2 + (z_3 - z_0)^2 = l^2 & \text{(iii)} \\ (x_4 - x_0)^2 + (y_4 - y_0)^2 + (z_4 - z_0)^2 = l^2 & \text{(iv)} \end{cases} \quad (36)$$

By subtracting Eq. (36)–(i) with Eq. (36)–(ii), Eq. (36)–(iii), Eq. (36)–(iv), we have

$$\begin{cases} x_0(x_2 - x_1) + y_0(y_2 - y_1) + z_0(z_2 - z_1) = \frac{(x_2^2 + y_2^2 + z_2^2) - (x_1^2 + y_1^2 + z_1^2)}{2} \\ x_0(x_3 - x_1) + y_0(y_3 - y_1) + z_0(z_3 - z_1) = \frac{(x_3^2 + y_3^2 + z_3^2) - (x_1^2 + y_1^2 + z_1^2)}{2} \\ x_0(x_4 - x_1) + y_0(y_4 - y_1) + z_0(z_4 - z_1) = \frac{(x_4^2 + y_4^2 + z_4^2) - (x_1^2 + y_1^2 + z_1^2)}{2} \end{cases} \quad (37)$$

which can be described as $\mathbf{P} \cdot \mathbf{S}_c = \mathbf{b}$:

$$\mathbf{P} = \begin{bmatrix} (x_2 - x_1) & (y_2 - y_1) & (z_2 - z_1) \\ (x_3 - x_1) & (y_3 - y_1) & (z_3 - z_1) \\ (x_4 - x_1) & (y_4 - y_1) & (z_4 - z_1) \end{bmatrix}, \quad (38)$$

$$\mathbf{b} = \begin{bmatrix} \frac{(x_2^2 + y_2^2 + z_2^2) - (x_1^2 + y_1^2 + z_1^2)}{2} \\ \frac{(x_3^2 + y_3^2 + z_3^2) - (x_1^2 + y_1^2 + z_1^2)}{2} \\ \frac{(x_4^2 + y_4^2 + z_4^2) - (x_1^2 + y_1^2 + z_1^2)}{2} \end{bmatrix}, \quad (39)$$

$$\mathbf{S}_c = (x_0 \ y_0 \ z_0)^T, \quad (40)$$

where the matrix \mathbf{P} means is three non-coplanar vectors or lines such that any one of the three lines cannot be described by the other two. Thus, the rank of \mathbf{P} is 3 and $\det(\mathbf{P}) \neq 0$. Therefore, according to *Cramer's Rule* [59], we can get a unique solution for $\mathbf{P} \cdot \mathbf{S}_c = \mathbf{b}$.

Proof end.

ACKNOWLEDGEMENT

The authors would like to thank the Pointing'04 ICPR Workshop and the Computer Vision Laboratory of ETH Zurich providing the database for head pose estimation.

REFERENCES

- [1] E. M. Chutorian, A. Doshi, and M. M. Trivedi, "Head pose estimation for driver assistance systems: A robust algorithm and experimental evaluation," in *Proc. IEEE Intell. Transp. Syst. Conf.*, Sep. 2007, pp. 709–714.
- [2] E. M. Chutorian and M. M. Trivedi, "Head pose estimation and augmented reality tracking: an integrated system and evaluation for monitoring driver awareness," *IEEE Transactions on Intelligent Transportation Systems*, vol. 11, no. 2, pp. 300–311, Jun. 2010.

- [3] X. Fu, X. Guan, E. Peli, H. Liu, and G. Luo, “Automatic calibration method for driver’s head orientation in natural driving environment,” *IEEE Transactions on Intelligent Transportation Systems*, vol. 14, no. 1, pp. 303–312, Mar. 2013.
- [4] A. Narayanan, R. M. Kaimal, and K. Bijlani, “Estimation of driver head yaw angle using a generic geometric model,” *IEEE Transactions on Intelligent Transportation Systems*, vol. 17, no. 12, pp. 3446–3460, Dec. 2016.
- [5] R. O. Mbouna, S. G. Kong, and M. G. Chun, “Visual analysis of eye state and head pose for driver alertness monitoring,” *IEEE Transactions on Intelligent Transportation Systems*, vol. 14, no. 3, pp. 1462–1468, Sep. 2013.
- [6] L. Fridman, J. Lee, B. Reimer, and T. Victor, “‘‘Owl’’ and ‘‘Lizard’’: Patterns of head pose and eye pose in driver gaze classification,” *IET Computer Vision*, vol. 10, no. 4, 308–313, Jul. 2016.
- [7] A. Tawari, S. Martin, and M. M. Trivedi, “Continuous Head Movement Estimator (CoHMET) for driver assistance: Issues, algorithms and on-road evaluations,” *IEEE Transactions on Intelligent Transportation Systems*, vol. 15, no. 2, pp. 812–824, Apr. 2014.
- [8] T. Bar, J. F. Reuter, and J. M. Zollner, “Driver head pose and gaze estimation based on multi-template ICP 3-D point cloud alignment,” in *Proc. IEEE Conf. Intell. Transp. Syst.*, pp. 1797–1802, Sep. 2012.
- [9] G. A. Peláez C., F. García, A. de la Escalera, and J. M. Armingol, “Driver monitoring based on low-cost 3-d sensors,” *IEEE Transactions on Intelligent Transportation Systems*, vol. 15, vo.4, pp. 1855–1860, Aug. 2014.
- [10] J. P. Batista, “A real-time driver visual attention monitoring system,” in *Proc. Iberian Conference on Pattern Recognition and Image Analysis, Lecture Notes in Computer Science*, vol. 3522, pp. 200–208, 2005.
- [11] M. Cohen, I. Shimshoni, E. Rivlin, and A. Adam, “Detecting mutual awareness events,” *IEEE Transactions on Pattern Analysis and Machine Intelligence*, vol. 34, no. 12, pp. 2327–2340, 2012.
- [12] R. Valenti, N. Sebe, and T. Gevers, “Combining head pose and eye location information for gaze estimation,” *IEEE Transactions on Image Processing*, vol. 21, no. 2, pp. 802–815, Feb. 2012.
- [13] J. Li and S. Li, “Gaze estimation from color image based on the eye model with known head pose,” *IEEE Transactions on Human-Machine Systems*, vol. 46, no. 3, pp. 414–423, Jun. 2016.
- [14] S. Duffner and C. Garcia, “Visual focus of attention estimation with unsupervised incremental learning,” *IEEE Transactions on Circuits and Systems for Video Technology*, vol. 26, no. 12, pp. 2264–2272, Dec. 2016.
- [15] A. Riener and A. Sippl, “Head-pose-based attention recognition on large public displays,” *IEEE Computer Graphics and Applications*, vol. 34, no. 1, pp. 32–41, Jan. 2014.
- [16] S. O. Ba and J.-M. Odobez, “Multiperson visual focus of attention from head pose and meeting contextual cues,” *IEEE Transactions on Pattern Analysis and Machine Intelligence*, vol. 33, no. 1, pp. 101–1116, Jan. 2011.
- [17] N. M. Bakker, Boris A. J. Lenseigne, “Accurate gaze direction measurements with free head movement for strabismus angle estimation,” *IEEE Transactions on Biomedical Engineering.*, vol. 60, no. 11, pp. 3028–3034, Nov. 2013.
- [18] H. Proen  a, J. C. Neves, S. Barra, T. Marques, and J. C. Moreno, “Joint head pose/soft label estimation for human recognition in-the-wild,” *IEEE Transactions on Pattern Analysis and Machine Intelligence*, Vol. 38, no. 12, pp. 2444–2456, Dec. 2016.
- [19] H. M. Takallou and S. Kasaei, “Head pose estimation and face recognition using a non-linear tensor-based model,” *IET Computer Vision*, vol. 8, no. 1, pp. 54–65, Feb. 2014.
- [20] S. M. LaValle, A. Yershova, M. Katsev and M. Antonov, “Head tracking for the Oculus Rift,” in *Proc. IEEE International Conference on Robotics and Automation (ICRA)*, pp. 187–194, 2014.
- [21] E. R. van Kesteren, J. P. van Maanen, A. A. J. Hilgevoord, D. M. Laman, N. de Vries, “Quantitative effects of trunk and head position on the apnea hypopnea index in obstructive sleep apnea,” *Sleep*, vol. 34, no. 8, pp. 1075–108, Aug. 2011.
- [22] E. Sariyanidi, H. Gunes, and A. Cavallaro, “Automatic analysis of facial affect: A survey of registration, representation, and recognition,” *IEEE Transactions on Pattern Analysis and Machine Intelligence*, vol. 37, no. 6, pp. 1113–1133, Jun. 2015.
- [23] D. Dervinis, “Head orientation estimation using characteristic points of face,” *Electronics and Electrical Engineering*, vol. 72, no.8, pp. 61-64, Jan. 2006.
- [24] E. M. Chutorian and M. M. Trivedi, “Head pose estimation in computer vision: A survey,” *IEEE Transactions on Pattern Analysis and Machine Intelligence*, vol. 31, no. 4, pp. 607–626, Apr. 2009.
- [25] D. J. Tan, F. Tombari, and N. Navab, “Real-Time accurate 3d head tracking and pose estimation with

consumer RGB-D cameras," *International Journal of Computer Vision*, pp. 1-26, 2017.

[26] G. Fanelli, M. Dantone, J. Gall, A. Fossati, L. V. Gool, "Random forests for real time 3d face analysis," *International Journal of Computer Vision*, vol. 101, no. 3, pp. 437–458, Feb. 2013.

[27] H. Liang, J. Hou, J. Yuan, and D. Thalmann, "Random forest with suppressed leaves for hough voting," in *Proc. ACCV'16*, pp. 264-280, Nov. 2016.

[28] S. S. Mukherjee and N. M. Robertson, "Deep head pose: gaze-direction estimation in multimodal video," *IEEE Transactions on Multimedia*, vol. 17, no. 11, pp. 2094–2107, Nov. 2015.

[29] M. Venturelli, G. Borghi, R. Vezzani, and R. Cucchiara, "From depth data to head pose estimation: a siamese approach," in *Proc. International Joint Conference on Computer Vision, Imaging and Computer Graphics Theory and Applications (VISIGRAPP)*, Porto, Portugal, Mar. 2017.

[30] V. Drouard, R. Horaud, A. Deleforge, S. Ba, and G. Evangelidis, "Robust head-pose estimation based on partially-latent mixture of linear regressions," *IEEE Transactions on Image Processing*, vol. 26, no. 3, pp. 1428–1440, Mar. 2017.

[31] Y. Li, S. Wang, and X. Ding, "Person-independent head pose estimation based on random forest regression," in *Proc. IEEE International Conference on Image Processing (ICIP)*, pp. 1521-1524, Sep. 2010.

[32] X. Liu, W. Liang, Y. Wang, S. Li, and M. Pei, "3D head pose estimation with convolutional neural network trained on synthetic images," in *Proc. IEEE International Conference on Image Processing (ICIP)*, pp. 1289–1293, Sep. 2016.

[33] A. K. Rajagopal, R. Subramanian, E. Ricci, et al. "Exploring transfer learning approaches for head pose classification from multi-view surveillance images," *International Journal of Computer Vision*, pp. 146-167, Aug. 2014.

[34] J. Foytik, and V. K. Asari, "A two-layer framework for piecewise linear manifold-based head pose estimation," *International journal of computer vision*, vol. 101, no. 2, pp. 270–287, Jan. 2013.

[35] S. Asteriadis, K. Karpouzis, and S. Kollias, "Visual focus of attention in non-calibrated environments using gaze estimation," *International Journal of Computer Vision*, vol. 107, no. 3, pp. 293–316, May 2014.

[36] A. Sadeghzadeh, H. Ebrahimnezhad, "Head pose estimation based on fuzzy systems using facial geometric features," in *Proc. 8th International Symposium on Telecommunications (IST)*, pp. 777-782, Sep. 2016.

[37] G. Riegler, D. Ferstl, M. Rüther and H. Bischof, "Hough networks for head pose estimation and facial feature localization," in *Proceedings British Machine Vision Conference*, 2014.

[38] C. Papazov, T. K. Marks, and M. Jones, "Real-time 3d head pose and facial landmark estimation from depth images using triangular surface patch features," in *Proc. IEEE Conference on Computer Vision and Pattern Recognition*, pp. 4722–4730, Jun. 2015.

[39] A. Gee and R. Cipolla, "Determining the gaze of faces in images," *Image and Vision Computing*, vol. 12, no. 10, pp. 639-647, 1994.

[40] Q. Ji and R. Hu, "3D face pose estimation and tracking from a monocular camera," *Image and Vision Computing*, vol. 20, no. 7, pp. 499–511, May 2002.

[41] P. Yao, G. Evans, A. Calway, "Using affine correspondance to estimate 3-d facial pose," in *Proc. IEEE International Conference on Image Processing (ICIP)*, pp. 919-922, Oct. 2001.

[42] A. Narayanan, R. M. Kaimal, and K. Bijlani, "Yaw estimation using cylindrical and ellipsoidal face models," *IEEE Transactions on Intelligent Transportation Systems*, vol. 15, no. 5, pp. 2308–2320, Oct. 2014.

[43] A. Nikolaidis, and I. Pitas, "Facial feature extraction and pose determination," *Pattern Recognition*, vol. 33, no. 11, pp. 1783–1791, Nov. 2000.

[44] J. Xiao, S. Baker, I. Matthews, and T. Kanade, "Real-time combined 2D+3D active appearance models," in *Proc. IEEE Conference on Computer Vision and Pattern Recognition*, vol. 2, pp. 535–542, Jun. 2004.

[45] P. Martins and J. Batista, "Single view head pose estimation," in *Proc. IEEE International Conference on Image Processing (ICIP)*, pp. 1652–1655, Oct. 2008.

[46] M. Martin, F. Van De Camp, and R. Stiefelhagen, "Real time head model creation and head pose estimation on consumer depth cameras," in *Proc. International Conference on 3D Vision*, pp. 641–648, Dec. 2014.

[47] S. Li, K. N. Ngan, R. Paramesran, and L. Sheng, "Real-Time head pose tracking with online face template reconstruction," *IEEE Transactions on Pattern Analysis and Machine Intelligence*, vol. 38, no. 9, pp. 1922–1928, Sep. 2016.

[48] G. P. Meyer, S. Gupta, I. Frosio, D. Reddy, and J. Kautz, "Robust model-based 3d head pose estimation,"

in *Proc. IEEE International Conference on Computer Vision (ICCV)*., pp. 3649–3657, Dec. 2015.

[49] S. G. Kong, and R. O. Mbouna, “Head pose estimation from a 2d face image using 3d face morphing with depth parameters,” *IEEE Transactions on Image Processing*, vol. 24, no. 6, pp. 1801–1808, Jun. 2015.

[50] Z. Zhang, “A flexible new technique for camera” *IEEE Transactions on Pattern Analysis and Machine Intelligence*, vol. 22, no. 11, pp. 1330–1334, Nov. 2000.

[51] G. Wang, Q. M. J. Wu, *Simplified Camera Projection Models*, London: Springer Press. 2011, pp. 30–32.

[52] J. J. More, “The levenberg-marquardt algorithm: implementation and theory,” in *Proc. Conference on Numerical Analysis*, Dundee, UK, 28, Jun 1977

[53] N. Gourier, D. Hall, and J. Crowley, “Estimating face orientation from robust detection of salient facial structures,” in *Proc. Pointing 2004, ICPR, International Workshop on Visual Observation of Deictic Gestures*, pp. 17-25, Aug. 2004.

[54] BIWI Kinect head pose database [Online], (2011). Available: http://www.vision.ee.ethz.ch/gfanelli/head_pose/head_forest.html#db.

[55] 3DSMAX (Autodesk, N.A). Accessed on Apr. 13, 2017. [Online]. Available: <https://www.autodesk.com/products/3ds-max>.

[56] D. Li, W. Pedrycz, “A centralprofile-based 3D face pose estimation,” *Pattern Recognition*, vol. 47, no. 2, pp. 525-534, Feb. 2014.

[57] Y. Sun, X. Wang, X. Tang, “Deep convolutional network cascade for facial point detection,” in *Proc. IEEE Conference on Computer Vision and Pattern Recognition*, pp.3476-3483, Jun. 2013.

[58] I. Matthews and S. Baker, “Active appearance models revisited,” *Int. J. Comput. Vis.*, vol. 60, no. 2, pp. 135–164, 2004.

[59] M. Thomas. The theory of determinants in the historical order of development, vol. 1. New York: Dover, pp. 11-14, 1960.

[60] J. Gu, X. Yang, S. D. Mello, and J. Kautz “Dynamic facial analysis: from bayesian filtering to recurrent neural network,” in *Proc. 30th IEEE Conference on Computer Vision and Pattern Recognition (CVPR2017)*, pp. 1531-1540, Jul. 2017.

[61] S. Lathuilière, R. Juge, P. Mesejo, R. M.-Salinas, and R. Horaud, “Deep mixture of linear inverse regressions applied to head-pose estimation,” in *Proc. 30th IEEE Conference on Computer Vision and Pattern Recognition (CVPR2017)*, pp. 7149-7157, Jul. 2017.